PHOTOELECTRONICS

UDC 621.383.4/5
EDN: GYMBFM

PACS: 42.79.Pw, 85.60.Gz, 07.57.Kp, 85.60.Dw

MWIR focal plane array based on CdHgTe *n*B*n*-architecture with superlattice barrier layer

K. O. Boltar, I. D. Burlakov, N. I. Iakovleva, M. V. Sednev, A. V. Trukhachev, N. A. Irodov, A. A. Lopukhin, E. V. Permikina, A. V. Voitsekhovskii, D. I. Gorn, N. N. Mikhailov

Medium wavelength IR focal plane array (FPA) based on CdHgTe nBn-architecture with superlattice barrier layer has been developed and investigated. The FPA consists of 64×64 elements with 40 µm pith, hybridized with silicon readout integrated circuit (ROIC). The photosensitive assembly of FPA and ROIC was measured in a vacuum cryostat filling liquid nitrogen. The spectral and photoelectric parameters of CdHgTe FPAs based on nBn architecture with superlattice barrier layer have been measured under optimal bias conditions. The average detectivity value was of $D^{*} \sim 7\times10^{10}$ cmW^{-1}Hz$^{1/2}$, the average voltage sensitivity value was of $S_u \sim 6\times10^{7}$ V/W.

Keywords: FPA, *n*B*n,* heterostructure; MWIR; HgCdTe; MCT; photosensitive element; spectral response.

DOI: 10.51368/1996-0948-2025-1-38-44

1. Introduction

The development of epitaxial growth methods of $Cd_xHg_{1-x}Te$ material, primarily molecular beam epitaxy (MBE), has enabled to solve a number of technological problems in creating high-operating-temperature focal plane arrays (FPAs) and photodetectors [1, 2], including the development of design and topology for CdHgTe multilayer barrier heterostructures with superlattices as the barrier.

The layer with a unipolar conductivity type, forming *n*B*n* heterostructures, ensure the minimal dark currents of photosensitive elements [3–5]. Based on *n*B*n* heterostructure FPAs with photosensitive elements, separated by the mesa-etching method to individual elements, do not contain any *p*-type regions, while the array elements operate like ordinary photodiodes, by applying bias to the base and contact layers.

The development of new barrier architectures based on CdHgTe unipolar *n*B*n* heterostructures including superlattices as the barrier for MWIR and LWIR FPAs and photodetectors, is considered as a very important problem [6, 7], which solving could improve the production of new type devices with a small number of defects, increase operating temperature and make better performance.

The paper discusses the concept of MWIR FPA design based on CdHgTe *n*B*n* heterostructure with superlattice as a barrier. CdHgTe FPAs with various topologies including absorbing *n*-layers were manufactured on the basis of barrier *n*B*n* heterostructures with superlattices as a barriers. The spectral and photovoltaic characteristics of MWIR CdHgTe devices based on *n*B*n* heterostructures with superlattices as barriers have been investigated.

2. Architecture of CdHgTe-based *n*B*n* barrier structures

$Cd_xHg_{1-x}Te$ multilayer *n*B*n* heterostructures were grown using the MBE method on optically transparent GaAs (013) substrates at the Institute of Semiconductor Physics of the Siberian Branch of the Russian Academy of Sciences [8, 9]. A ZnTe buffer layer (~ 30 nm), a relaxing CdTe buffer layer (5.5 μm), and a graded-gap $Cd_xHg_{1-x}Te$ layer (1 μm) were successively formed on the substrate. The active working region of the $Cd_xHg_{1-x}Te$ *n*B*n* structure consisted of an absorbing layer, a barrier layer, and a contact layer (Fig. 1). The absorbing $Cd_xHg_{1-x}Te$ layer was of approximately 3–4 μm thickness. The CdTe composition in the barrier layer and in the contact layer of ~ 1 μm thickness has been selected in accordance with the operating spectral range.

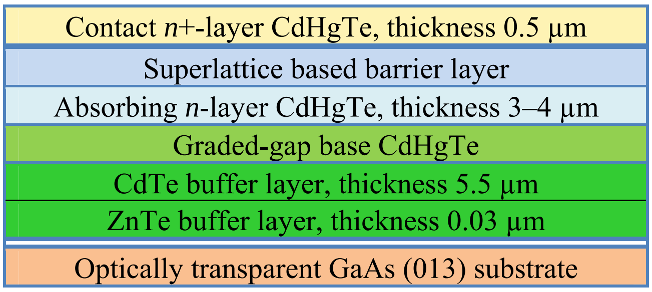

Fig. 1. Layer-by-layer configuration of CdHgTe nBn-barrier structure with a superlattice

The layer-by-layer configuration of MWIR CdHgTe barrier *n*B*n* structure with a superlattice is presented in Table 1.

Table 1

Parameters of layers of nBn heterostructure based on CdHgTe

Name of the layer in the structure	Concentration, cm^{-3}	Composition, mole fraction	Thickness, μm
n-$Cd_xHg_{1-x}Te$ contact layer	$n \sim (1–3)\times10^{16}$	0.3	0.5
n-$Cd_xHg_{1-x}Te$ contact layer	–	0.03 (well) / 0.75 (barrier).	0.004 (barrier) / 0.010 (well); 10 periods 0.140 (total)
$Cd_xHg_{1-x}Te$ absorbing *n*-layer	$n \sim (3–5)\times10^{15}$	0.3	3.0–4.0
Graded-gap base CdHgTe	–	1.0–0.3	1.0
CdTe buffer layer	–	–	5.5
ZnTe buffer layer	–	–	0.03
GaAs (013) substrate, ∅ 50.8 mm			600

During the growing process, the doping of the working area was carried out with a donor indium impurity, the concentration of the impurity in the absorbing and barrier layers was approximately the same, and in the contact layer it was several times higher.

The composition profile of the CdHgTe *n*B*n* heterostructure with the barrier region consisting of 10-period superlattice, is shown in Fig. 2.

As shown in Figure 2, in the $Cd_xHg_{1-x}Te$ multilayer heterostructure, from left to right starting from the absorbing layer of composition $x = 0.28$ mole fraction, there is a 10-periods superlattice consisting of HgTe/$Cd_xHg_{1-x}Te$ layers, while the wide-band layer is $Cd_xHg_{1-x}Te$ of composition $x = 0.72$ mole fraction, the well layer is formed by a semi-metallic HgTe binary compound, the barrier layer is approximately 4 times smaller thickness than the HgTe layer, and a contact layer of composition $x = 0.3$ mole fraction is grown on top of the barrier layer.

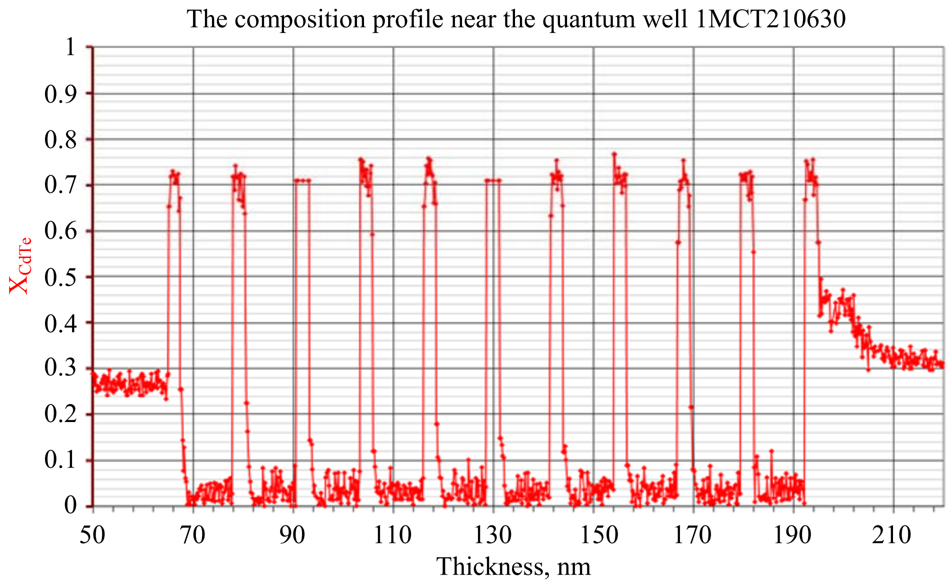

Fig. 2. The composition profile in the CdHgTe nBn heterostructure with the 10-period superlattice barrier.

3. Research and discussion of results

MWIR FPAs and matrix photodetectors were fabricated on the basis of CdHgTe *nBn* heterostructures with superlattices as the barrier. The 64×64 format with a 40 μm pitch arrays of photosensitive elements were formed using mesa-etching method. The crystal with the 64×64 element array had overall dimensions of ~2.74×2.74 mm (Fig. 3*a*). The local size of the contact *n*-region was 0.02×0.02 mm, and an ohmic In microcontacts were fabricated for each photosensing element by photolithography method.

A silicon ROIC (Fig. 3*b*) intending for reading, pre-analog processing and output signals from a 64×64 element array provided an accumulation of photocurrent on integrating capacitors and multiplexing of signals into 2 analog outputs. The hybrid assembly of FPA and ROIC obtained by the flip-chip method was located in a vacuum cryostat for detecting a photosignal at an operating temperature of $T = 77$ K.

The current-voltage characteristics of test array elements were measured at $T = 300$ K (Fig. 4), and the relative spectral response have been measured at $T = 77$ K (Fig. 5).

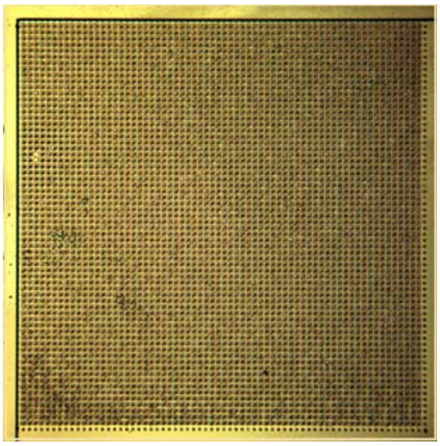

a) FPA

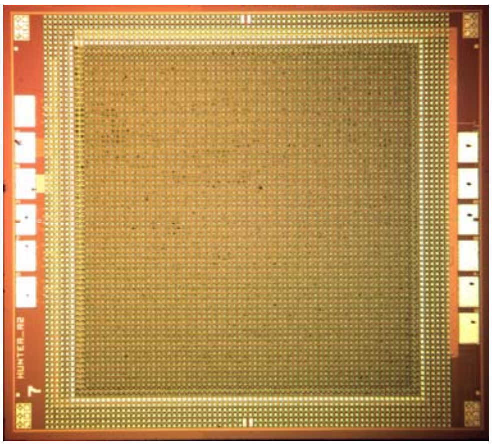

b) 64×64 element ROIC

Fig. 3. 64×64 element with 40 µm pitch FPA and 64×64 element ROIC

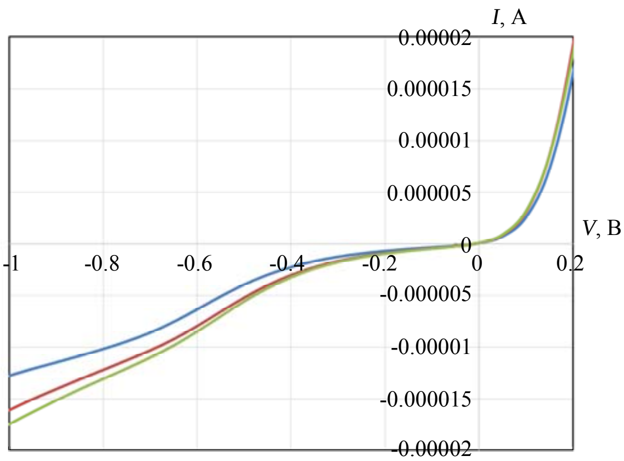

Fig. 4. Current-voltage characteristics of test elements of a 64×64 element FPA with of 40 µm pitch for the MWIR spectral range (3–5 µm) at T = 300 K

The current-voltage characteristic of MWIR FPA (Fig. 4) differs from current-voltage characteristic of n/p photodiode due to its unipolar nature. The presented current-voltage characteristic under forward bias voltage determines the dark current generated in the collector volume, while under reverse bias voltage, it is generated in the base layer volume. In the absorption region, the doping level was of $N_d \sim 3\times10^{15}$ cm^{-3}, the lifetime was of $\sim10^{-5}$ s, and the absorption region thickness was of ~3–4 µm. The flat-band voltage was approximately $V_{fb} \approx -0.2$ V. The generation-recombination current in the depletion region appeared at bias voltages $V > V_{fb}$, while the tunneling current occurred at bias voltages $V > V_{fb} + E_g \approx (0.2 + 0.25)$ V. The tunneling mechanism is caused by traps with a trap concentration of approximately $N_t \sim 10^{11}$ cm^{-3}.

The components of the dark current for the FPA based on an *n*B*n* structure with a barrier layer are identical to the current components that determine the behavior of charge carriers in a photodiode, except for the tunneling current, which changes due to the presence of the barrier (it is small at low biases but increases with higher bias voltages).

The relative spectral response of the test PSE at T = 77 K is shown in Figure 5.

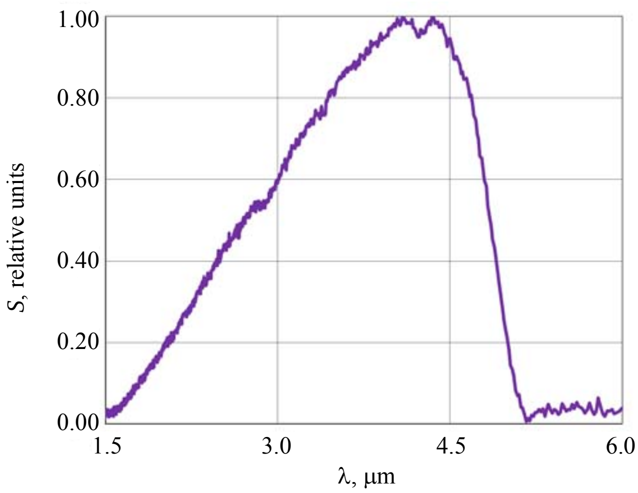

Fig. 5. Relative spectral response of the test array element at T = 77 K, λ_{gr} = 4.88 µm

The long-wavelength cutoff of the spectral response at a 0.5 level for MWIR FPA was of λ_{gr} = 4.88 µm, it was formed by the choice of the $Hg_{1-x}Cd_xTe$ composition, and the short-wavelength cutoff at a 0.5 level was of λ_k = 2.72 µm, that determined by the absorption of radiation in the graded-gap layer of the *n*B*n* heterostructure with ~ 1 µm thickness.

To measure the performance of 64×64 FPA with a 40 µm pitch based on *n*B*n* heterostructures, an computer-aided and processing system was used, which allowed to the automatic measurement of the noise and photosignal voltages of each array element and the following performance calculation. Measurements of the photosignal and noise voltages of MWIR FPA were carried out; the distributions of the photosignal and noise are presented in Figure 6 *a*, *b*.

The performance of the 64×64 MWIR FPA with 40 µm pitch based on CdHgTe *n*B*n* heterostructures were compared with the performance of the InSb FPA based on bulk material with a relative aperture of the cooled diaphragm of 1:0.9 (Table 2).

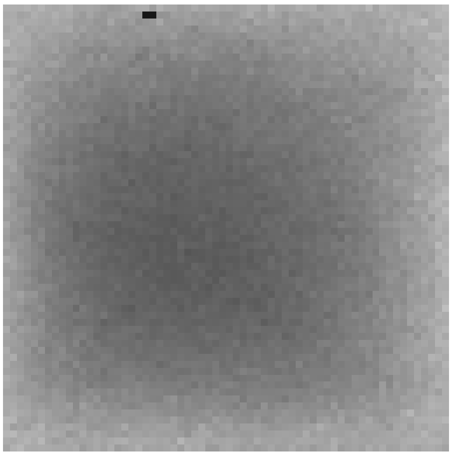

a) distribution of photosignal at *T* = 77 K

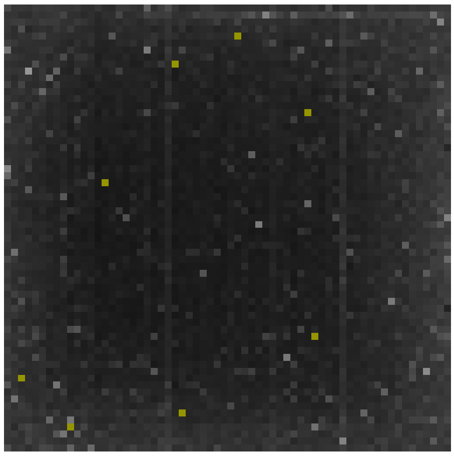

b) distribution of noise at *T* = 77 K

Fig. 6. Signal and noise distributions of the MWIR 64×64 FPA with 40 µm pitch based on the HgCdTe nBn heterostructure

Table 2

Performances of the 64×64 FPAs with 40 µm pitch

FPA No.	Integration time, µs	Cutoff wavelength, µm	Volt sensitivity, S_u, V/W	Detectivity D^*, cm·Hz$^{1/2}$·W^{-1}
FPA1	99	4.88	5.2×10^7	6.7×10^{10}
FPA2	99	4.92	6.4×10^7	7.4×10^{10}
FPA-InSb	120	5.48	1.0×10^8	8.8×10^{10}

From the table and graphs it is evident that the diagrams of distribution of signal and noise voltage for 64×64 arrays, as well as the average values of the main performance, confirm the possibility of creating FPAs and PDs based on HgCdTe *n*B*n* heterostructures with superlattices as a barrier. The low values of the detectivity, obtained at the first stage of the research, indicate the need to redesign and the further development of the technology both in mesa-array passivation and in growing HgCdTe *n*B*n* heterostructures with wide-gap barriers.

4. Conclusion

Using the molecular beam epitaxy method, CdHgTe multilayer *n*B*n* heterostructures with an absorbing *n*-layers and with superlattices as a barriers were obtained for the production of focal plane arrays of a new design and topology. The photodetectors and 64×64 FPAs and with 40 μm pitch have been manufactured and investigated.

The current-voltage characteristics of the test elements of MWIR FPAs at the low-voltage bias were measured at normal climatic conditions. The results of the current-voltage characteristic measurements at T = 300 K showed that the components of the dark current for a FPA based on an *n*B*n* structure with a barrier layer are identical to the components that determine the behavior of charge carriers in a *p*/*n* photodiode, except for the tunnel current, which changes under the influence of the barrier layer. The spectral responses of the MWIR FPAs with a long-wave cutoff of $\lambda_{0.5} \sim 4.9$ μm, which corresponds to the atmospheric transparency window.

The average value of detectivity for the FPA1 was of $D^*_1 = 6.7\times10^{10}$ cm·W^{-1}·Hz$^{1/2}$. The average value of the volt sensitivity S_u for the FPA1 was of $S_{u1} = 5.2\times10^7$ V/W. The average value of detectability for the FPA2 was $D^*_1 = 7.4\times10^{10}$ cm·W^{-1}·Hz$^{1/2}$. The average value of the volt sensitivity S_u for the FPA2 was $S_{u2} = 6.4\times10^7$ V/W. The difference in number of defects and detectivity values D^* for different FPAs are connected with the quality of FPA surface passivation. To improve the performance, further development of the technology both in FPA production and in growth processes improvement of HgCdTe *n*B*n* heterostructures with a superlattice as a barrier are required.

The study was supported by a grant from the Russian Science Foundation No. 23-62-10021, https://rscf.ru/project/23-62-10021.

REFERENCES

1. Boltar K. O., Burlakov I. D., Iakovleva N. I., Vlasov P. V., and Lazarev P. S., Usp. Prikl. Fiz. (Advances in Applied Physics) **10** (2), 170–182 (2022) [in Russian].
2. Piotrowski J. and Rogalski A. High-Operating-Temperature Infrared Photodetectors, SPIE Press, Bellingham, 2007.
3. Izhnin I. I., Kurbanov K. R., Voitsekhovskii A. V., Nesmelov S. N., Dzyadukh S. M., Dvoretsky S. A., Mikhailov N. N. and Sidorov G. Y., Appl. Nanosci. **10**, 4571–4576 (2020).
4. Akhavan N. D., Umana-Membreno Gu. R., Antoszewski J. and Faraone L., IEEE Trans Electron. Dev. 65, 591–598 (2018).
5. Itsuno A. M., Phillips J. D. and Velicu S., Journal of Electronic Materials **40** (8), 1624–1629 (2011).
6. Voitsekhovskii A. V., Nesmelov S. N., Dzyadukh S. M., Vasil'ev V. V., Varavin V. S., Dvoretsky S. A., Mikhailov N. N., Yakushev M. V. and Sidorov G. Yu., Applied Physics, No. 4, 83–86 (2016) [in Russian].
7. Kopytko M. et al., J. Electron. Mater. **44** (1), 158–166 (2015).
8. Voitsekhovskii A. V., Nesmelov S. N., Dzyadukh S. M., Dvoretsky S. A., Mikhailov N. N., Sidorov G. Yu. and Yakushev M. V., Infr. Phys. and Techn. **102**, 103035 (1–4) (2019).
9. Varavin V. S., Sabinina I. V., Sidorov G. Yu., Marin D. V., Remesnik V. G., Predein A. V., Dvoretsky S. A., Vasilyev V. V., Sidorov Yu. G., Yakushev M. V. and Latyshev A. V., Infrared Phys. Technol. **105**, 103182 (2020). doi: 10.1016/j.infrared.2019.103182.

Konstantin O. Boltar[1,2], Head of Scientific and Technical Complex, Doctor of Physical and Mathematical Sciences, Professor
Igor D. Burlakov[1,3], Deputy Director General for Innovations and Science, Doctor of Technical Sciences, Professor
Natalia I. Iakovleva[1], Chief Staff Scientist, Doctor of Technical Sciences
E-mail: niiakovleva@mail.ru
Mikhail V. Sednev[1], Head of the Site, Candidate of Technical Sciences
Anton V. Trukhachev[1], Lead Engineer
Nikita A. Irodov[1], Head of the Site
Alexey A. Lopukhin[1], Head of the Site, Candidate of Technical Sciences
Elena V. Permikina[1], Lead Process Engineer
Alexandr V. Voytsekhovsky[4], Head of Department, Doctor of Physical and Mathematical Sciences
Dmitry I. Gorn[4], Head of the Laboratory, Candidate of Physical and Mathematical Sciences
E-mail: gorn_dim@sibmail.com
Nikolay N. Mikhaylov[5], Senior Staff Scientist, Candidate of Physical and Mathematical Sciences

[1] RD&P Center ORION, join-stock company
9, Kosinskaya st., Moscow, 111538 Russia
[2] Moscow Institute of Physics and Technology
9, Institutskiy lane, Dolgoprudny, Moscow region, 141701 Russia
[3] MIREA – Russian Technological University
78, Vernadskogo Ave., Moscow, 119454 Russia
[4] Tomsk State University
36, Lenina st., Tomsk, 634050 Russia
[5] Rzhanov Institute of Semiconductor Physics of the Siberian Branch of the Russian Academy of Sciences
13, Akademika Lavrentyeva Ave., Novosibirsk, 630090 Russia

Received December 12, 2024
Revised December 27, 2024
Accepted February 7, 2025
Scientific specialty code: 1.3.11